



ARTICLE

Identification and Characterization of a Novel Yellow Leaf Mutant *yl1* in Rice

Xiaofang Zeng^{1, #}, Guangzheng Li^{1, #}, Nu'an Liu², Yan Li¹, Jianrong Li¹, Xiaozhen Huang¹ and Degang Zhao^{1, 2, *}

¹Key Laboratory of Plant Resources Conservation and Germplasm Innovation in Mountainous Region, Ministry of Education, Institute of Agro-Bioengineering and College of Life Sciences, Guizhou University, Guiyang, 550025, China

²Guizhou Plant Conservation Technology Center, Guizhou Key Laboratory of Agricultural Biotechnology, Guizhou Academy of Agricultural Sciences, Guiyang, 550006, China

*Corresponding Author: Degang Zhao. Email: dgzhao@gzu.edu.cn

#These authors contributed equally to this study

Received: 02 January 2022 Accepted: 03 March 2022

ABSTRACT

Leaf-color mutants play an important role in the study of chlorophyll metabolism, chloroplast development, and photosynthesis system. In this study, the *yellow leaf 1* (*yl1*) rice mutant was identified from the ethyl methane sulfonate-treated mutant progeny of Lailong, a glutinous *japonica* rice landrace cultivated in Guizhou Province, China. Results showed that *yl1* exhibited yellow leaves with decreased chlorophyll content throughout the growth period. Chloroplast development in the *yl1* mutant was disrupted, and the grana lamellae was loosely packed and disordered. RNA sequencing and real-time quantitative polymerase chain reaction (qRT-PCR) analysis revealed that the chlorophyll synthesis-related genes *OsCHLH*, *OsCHLM*, *OsCHLG*, *PORB*, and *YGL8*, as well as the chloroplast development-related genes *FtsZ*, *OsRpoTp*, and *RbcL*, were down-regulated in the *yl1* mutant. Genetic analysis revealed that the yellow leaf phenotype of *yl1* was controlled by recessive nuclear gene. By employing the MutMap method, the mutation responsible for the phenotype was mapped to a 6.17 Mb region between 17.34 and 23.51 Mb on chromosome 3. Two non-synonymous single-nucleotide polymorphisms (SNPs) located in the gene locus *LOC_Os03g31210* and *LOC_Os03g36760* were detected in this region. The two SNPs were further confirmed by PCR and Sanger sequencing. The expression patterns of the two candidate genes indicated that *LOC_Os03g36760* showed greater potential for functional verification. Subcellular protein localization revealed that the encoded product of *LOC_Os03g36760* was localized in the nucleus, cytoplasm, and plasma membrane. These results will be useful for further characterization and cloning of the *yl1* gene, and for research on the molecular mechanisms controlling biogenesis and chloroplast biochemical processes.

KEYWORDS

Rice; *yl1*; chlorophyll biosynthesis; map-based cloning

1 Introduction

Rice (*Oryza sativa* L.) is an important crop that is a staple food for more than half of the world's population [1]. It has been estimated that rice production must increase by 40% by 2030 to meet the demands of the growing population [2]. The pigment of leaves is normally primarily green, but abnormal biosynthesis and degradation of chlorophyll can change the pigment content and proportions, and lead to



alteration of the leaf-color phenotype. Leaf color has an important influence on photosynthesis, growth, and development in plants [3]. To date, more than 200 leaf-color rice mutants have been reported and at least 50 leaf-color genes have been cloned, and are distributed among all 12 chromosomes in rice. Mutation of genes participating in chloroplast development, the chlorophyll metabolism pathway, and associated regulatory genes affect chlorophyll synthesis, thus resulting in leaf-color mutants. More than 20 chlorophyll synthesis-related genes and 14 genes involved in chloroplast development have been cloned in rice [4–10].

In rice, *OsCHLH* encodes the H subunit of magnesium chelatase (Mg-chelatase), a crucial enzyme for chlorophyll synthesis and chloroplast development [11]. The *YGL7* and *OsChl9* genes encode the CHLD and CHLI subunits of Mg-chelatase, respectively. Mutations in these subunits reduce the activity of Mg-chelatase, resulting in a yellow-green leaf phenotype [4–6]. Mutation of *OsCRDI*, a gene encoding Mg-protoporphyrin IX monomethyl ester cyclase, causes abnormal chlorophyll synthesis and chloroplast development, resulting in a yellow leaf and dwarf phenotype in rice [12]. The genes *OsCAOI/PGL* and *OsCAO2* catalyze the synthesis of chlorophyll *b* from chlorophyll *a*. Of these two genes, *OsCAO1* plays a major role in the synthesis of chlorophyll *b*, whereas *OsCAO2* may play a less obvious role [7,13]. Protochlorophyllide oxidoreductase (POR) catalyzes the photoreduction of protochlorophyllide (Pchl_{id}) to chlorophyllide (Chl_{id}) during chlorophyll synthesis. The *OsPORB* gene is essential for maintenance of light-dependent chlorophyll synthesis, especially under high light intensity, whereas *OsPORA* functions mainly in the early stages of leaf development [14]. The *OsPORB* loss-of-function mutant *zgl16* shows a decreased pigment concentration and photosynthetic capacity [15].

Abnormal chloroplast development causes changes in the normal proportion and content of each chloroplast pigment, which is manifested as diverse leaf-color mutant phenotypes. Therefore, mutations in genes associated with the regulation of chloroplast development, such as *VYL (NAL9)*, *RNRL1 (V3)*, *OsNOA1/RIF1*, *OsGluRS*, and *ASL2*, may also cause leaf-color mutations [16–22]. Most proteins localized in chloroplasts are the coding products of nuclear genes. Thus, the mutation of genes involved in the regulation of signal transduction between chloroplasts and the nucleus may also cause a change in leaf color. In rice, *BGL* encodes a guanine nucleotide exchange factor, OsRopGEF10, which activates Rop/Rac GTPases. OsRopGEF10 acts as a molecular switch in signal transduction by substituting GTP (the active form) for bound GDP (the inactive form) in eukaryotic responses to external or internal signals. Mutation of *BGL* results in a bright green leaf phenotype [23]. In addition, a number of other associated genes regulate leaf color. *OsPDF1B* encodes peptide deformylase, which acts to remove the N-terminal formyl group from methionine residues in protein synthesis. The Pdf1b/Pdf1B homozygous mutant shows a degreening and growth-arrested phenotype with low chlorophyll content [24].

Studies of cloned rice leaf-color-associated genes have shown that such genes are involved in chlorophyll metabolism, chloroplast development, and chloroplast and nuclear signaling pathways. These results indicate that rice leaf color is regulated by a series of genes in multiple pathways. Gratifying progress has been made in elucidating the mechanism of rice leaf-color regulation, but leaf color development is a complex process, and the understanding of this regulatory network remains incomplete. Mutants are basic materials of genetic research and important materials for genomic research [25]. Leaf-color mutants are important in the study of photosynthesis, as well as morphogenesis of chloroplasts and other photosynthetic organs in response to environmental signals, and can possibly be used as screening markers in heterosis [26]. Therefore, the screening and identification of new leaf-color-related mutants, and gene mapping, cloning, and functional analysis of these mutants have important theoretical and practical applications in rice research.

In the current study, we isolated and characterized the *yellow leaf 1 (y11)* rice mutant from the ethyl methane sulfonate (EMS)-treated mutants of Lailong, a glutinous rice landrace grown in Guizhou

Province, China. The *yll* mutant exhibited a yellow leaf phenotype and reduced chlorophyll content throughout the growth period. Morphological observation and genetic analysis of the *yll* mutant, and fine mapping of the *yll* gene were performed, with the ultimate objective of cloning and functional analysis of the candidate gene.

2 Materials and Methods

2.1 Plant Materials and Growth Conditions

The *yellow leaf 1* (*yll*) rice mutant was isolated from the M₂ generation raised from EMS-treated seeds of Lailong, a glutinous rice landrace from Guizhou Province, China. The Lailong wild type (WT) and *yll* seeds were sown in a seedbed for 20 days and seedlings were transplanted to a paddy field in Guiyang, Guizhou Province. The mutants were differentiated from normal segregants by the yellow leaf phenotype. Morphological traits of the WT and *yll* mutant were recorded in the mature stage.

2.2 Transmission Electron Microscopic Analyses

For transmission electron microscopy, leaves from 30-day-old seedlings of the WT and *yll* mutant were cut into 5-mm-long pieces, fixed in 2.5% glutaraldehyde in phosphate buffer at 4°C for 4 h, rinsed, and incubated overnight in 1% OsO₄ solution at 4°C. The samples were subsequently dehydrated, embedded, sectioned, and stained as described by Wang et al. [8]. The sections were observed with a Hitachi H-7650 transmission electron microscope (Hitachi, Tokyo, Japan).

2.3 Pigment and Chlorophyll Precursor Determination

Pigments were extracted from fresh leaf tissue with 80% acetone. The absorbance of the extract was measured at 470, 645, and 663 nm with a Varioskan Flash spectrophotometer (Thermo Fisher Scientific, Waltham, MA, USA). Total chlorophyll, chlorophyll *a*, chlorophyll *b*, and carotene contents were determined following the method described by Arnon [27]. The content of δ -aminolevulinic acid (ALA) was measured based on the method of Morton [28]. The chlorophyll precursors protoporphyrin IX (Proto IX), magnesium-protoporphyrin IX (Mg-Proto IX), Pchl_{ide}, and Chl_{ide} were assayed following the previously described methods [29,30]. The chlorophyll precursors in the acetone phase were quantified with a Varioskan Flash spectrophotometer (Thermo Fisher Scientific, Waltham City, MA, USA) using Ex400:Em632 for Proto IX, Ex440:Em633 for Pchl_{ide}, Ex440:Em672 for Chl_{ide}, and Ex420:Em595 for Mg-Proto IX.

2.4 RNA-Sequencing Analysis and Real-Time Quantitative RT-PCR

Total RNA was extracted from leaves of 4-week-old *yll* and WT plants using an RNA extraction kit (Omega Bio-Tek, Doraville, GA, USA) in accordance with the manufacturer's instructions. The cDNA libraries were constructed and sequenced on a BGISEQ-500 platform by the Beijing Genomics Institute (Shenzhen, China; <http://www.genomics.org.cn>). Three biological replicates were prepared for each sequencing library. The DEGseq method was used to screen genes differentially expressed between groups [31]. The differentially expressed genes (DEGs) were selected according to a previously described method [32]. Clusters of orthologous groups (COG) functional classification, gene ontology (GO), and Kyoto Encyclopedia of Genes and Genomes (KEGG) metabolic pathways annotation and enrichment analyses were conducted by accessing the NCBI COG, GO, and KEGG databases, respectively.

For real-time quantitative RT-PCR (qRT-PCR), cDNAs were generated by RT-PCR using the High-Capacity cDNA Reverse Transcription Kit (Thermo Fisher Scientific, Waltham city, MA, USA). The qRT-PCR analyses were performed using an qTower3G Real-time PCR System (Analytik Jena AG, Jena City, Germany) and the SYBR[®] Green PCR Master Mix Kit (Thermo Fisher Scientific, Waltham City, MA, USA). The *OsActin1* gene was used as an internal reference to normalize the gene expression level.

The relative gene expression levels were calculated using the $2^{-\Delta\Delta Ct}$ method [33]. The primers used for real-time PCR are listed in Table S1.

2.5 Genetic Analysis and Map-Based Cloning of the *yll* Mutant

For genetic analysis, the *yll* mutant was crossed with two *indica* rice cultivars, ‘Yinguizhan’ and ‘9311’. The segregation of normal and yellow-leaved plants in the F₂ populations was investigated at the tillering stage. The mapping population was generated by crossing the *yll* mutant and WT to map the *yll* gene using the MutMap approach described as Abe et al. [34]. Genomic DNA bulks were prepared from the *yll* mutant Lailong, 20 yellow-leaved individuals, and 20 green-leaved plants from among the F₂ progeny. The DNA bulks were subjected to whole-genome sequencing using the Illumina HiSeq 2500 platform. The obtained reads were aligned to the reference Nipponbare genome (<http://rice.uga.edu/>) using SOAP2 software [35]. The single-nucleotide polymorphism (SNP) index was calculated as described by Abe et al. [34]. To identify the mutation sites of the *yll* alleles, we amplified the candidate genes using genomic DNA extracted from the WT and *yll* mutant. The amplified DNA fragment products were sequenced. The primers used for sequencing are listed in Table S1.

2.6 Protein Subcellular Localization

To determine the subcellular localization of the *LOC_Os03g36760* protein, the pCambia-35S-*LOC_Os03g36760*:GFP vector was constructed. *Agrobacterium tumefaciens* strain EHA105 harboring this vector was introduced into rice seedling protoplasts for transient expression following the method of Li et al. [36]. *Agrobacterium tumefaciens* strain EHA105 harboring the pCambia-35S:GFP vector was used as the control. The green fluorescent protein (GFP) fluorescence signal was observed with a laser confocal microscope (Leica SP8 STED, Leica Biosystems, Wetzlar City, Germany) under excitation at 488 nm.

2.7 Statistical Analysis

The statistical significance of differences in mean values of the examined parameters between the WT and *yll* mutant were determined using Student’s *t*-test as implemented in Microsoft Excel 2016 and PASW Statistics 18 (SPSS Inc., Chicago, IL, USA).

3 Results

3.1 Phenotype of the *yll* Mutant

The *yll* mutant was isolated from a pool of EMS-mutagenized progeny of the *japonica* glutinous rice landrace Lailong. The *yll* mutant exhibited a yellow leaf phenotype throughout the growth period (Figs. 1A–1D). No significant differences in tiller number, grain width, and grain thickness were observed between the *yll* mutant and WT (Table 1). Plant height, panicle length, flag leaf length, grain number per panicle, and 1000-grain weight of the *yll* mutant were significantly decreased compared with those of the WT. The effective grain number per spike, grain length, and 1000-grain weight of the *yll* mutant were 14.97%, 4.75%, and 5.66% lower than those of the WT, respectively (Table 1). These results indicated that mutation of the *yll* gene affected the yield.

3.2 Determination of Photosynthetic Pigment Content in the *yll* Mutant

To characterize the yellow leaf phenotype of the *yll* mutant, we determined the pigment content of the *yll* and WT at the seedling, tillering, and grain filling stages. The contents of chlorophyll *a*, chlorophyll *b*, and total chlorophyll of *yll* were significantly reduced at each growth stage compared with those of the WT (Figs. 2A–2C). The content of carotene in the *yll* mutant was significantly decreased at the seedling and tillering stages, but markedly increased at the grain filling stage (Figs. 2A–2C). No significant difference in chlorophyll *a* to chlorophyll *b* (Chl *a/b*) ratio was observed between the *yll* mutant and WT leaves at the seedling and tillering stages (Fig. 2D). The Chl *a/b* ratio of the *yll* mutant was 6.67% lower than that

of the WT at the grain filling stage. These data suggested that the yellow leaf phenotype of the *y11* mutant was the result of reduced photosynthetic pigment contents (Fig. 2D).

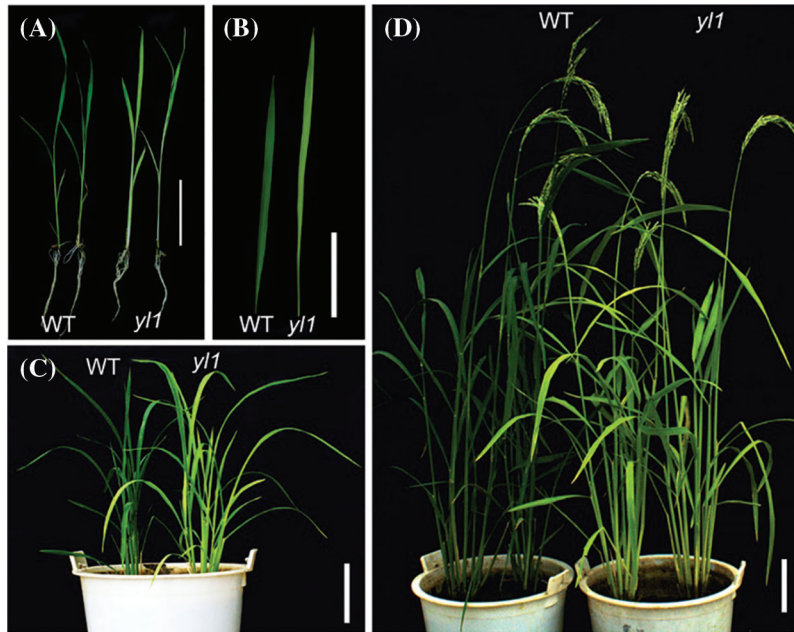


Figure 1: Rice leaf-color mutant *y11* and the wild type (WT) at different growth stages. A: Seedling stage, bar = 5 cm; B: seedling stage leaves, bar = 2 cm; C: tillering stage, bar = 10 cm; D: heading stage, bar = 10 cm

Table 1: Agronomic traits of the wild type (WT) and *y11* rice mutant

Trait	WT	<i>y11</i>
Plant height (cm)	145.82 ± 3.19	130.44 ± 3.28*
No. of tillers	12.00 ± 0.41	13.00 ± 1.58
Flag leaf length (cm)	36.16 ± 1.52	27.73 ± 1.55**
Panicle length (cm)	31.80 ± 0.96	24.88 ± 1.77**
No. of fertile seeds per panicle	215 ± 5.19	187 ± 8.67**
1000-grain weight (g)	31.57 ± 0.65	29.93 ± 0.45*
Unhulled seed (mm)		
Length	7.28 ± 0.17	6.95 ± 0.23*
Width	3.71 ± 0.09	3.70 ± 0.12
Thickness	2.59 ± 0.13	2.54 ± 0.04

Note: Data are the averages of 20 samples (± SD). * $P < 0.05$, ** $P < 0.01$.

To explore the affected pathway of chlorophyll synthesis in the *y11* mutant, the contents of chlorophyll intermediates were measured in the *y11* mutant and WT. No significant difference in the contents of ALA, porphobilinogen (PBG), uroporphyrinogen III (Urogen III), and coproporphyrinogen III (Coprogen III) were detected between the *y11* mutant and WT (Figs. 3A and 3B). However, the content of Proto IX in the *y11* mutant was significantly higher, and the contents of Mg-Proto IX and Pchlide were significantly decreased in the *y11* mutant, compared with those in the WT (Figs. 3B and 3C). These data indicated that the contents

of Mg-Proto IX and subsequent steps of chlorophyll synthesis in the *y11* mutant were significantly lower than those of the WT. It was speculated that the yellow leaf phenotype of the *y11* mutant was due to the reduction of chlorophyll content caused by impaired synthesis of Mg-Proxo IX. This hypothesis suggested that the *y11* mutant may be involved in chlorophyll biosynthesis at the Mg-Proto IX synthesis step.

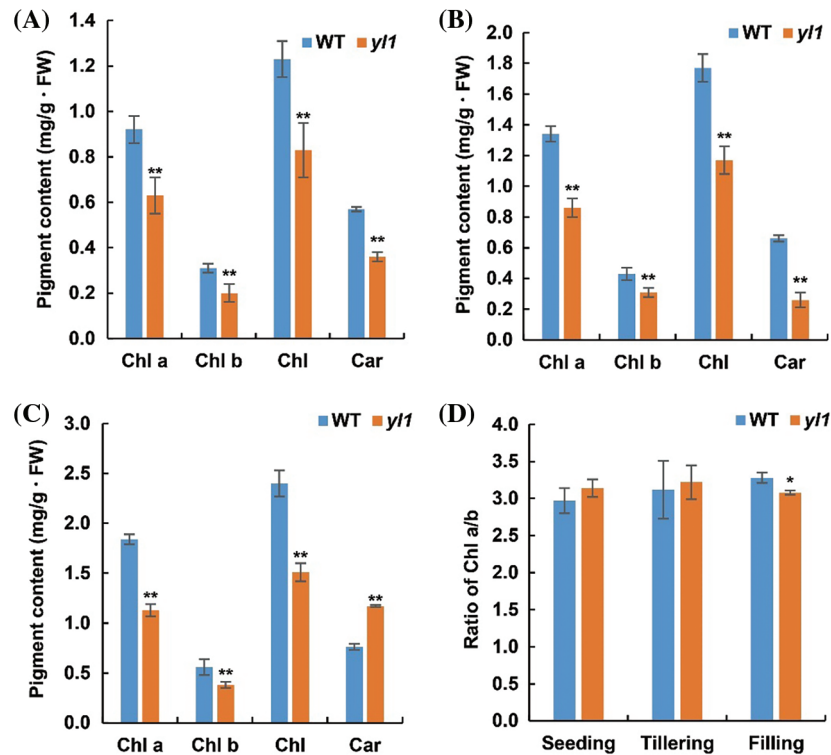


Figure 2: Photosynthetic pigment contents in the leaf of the *y11* mutant and wild type (WT) at three growth stages. A: Pigment contents at the seedling stage, B: pigment contents at the tillering stage, C: pigment contents at the grain filling stage, D: chlorophyll *a* to chlorophyll *b* ratio (Chl *a/b*) of the *y11* mutant and WT at the seedling, tillering, and grain filling stages. * $P < 0.05$, ** $P < 0.01$

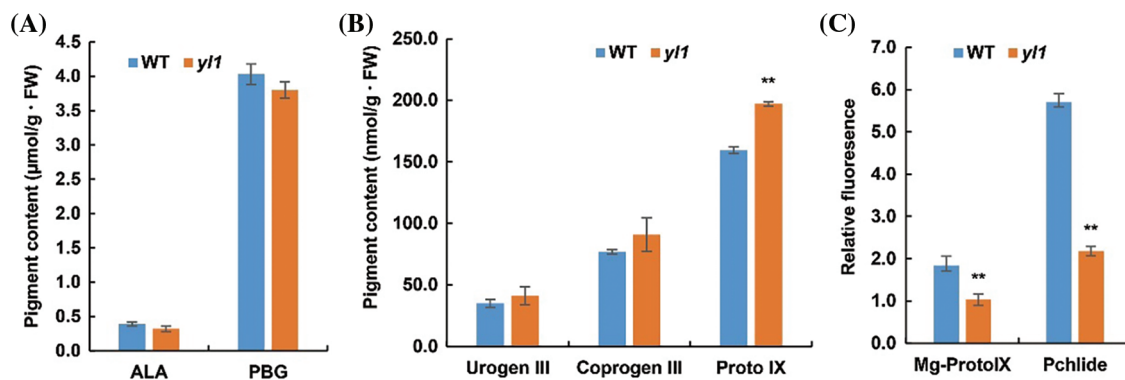


Figure 3: Contents of chlorophyll intermediates, and expression levels of chlorophyll biosynthetic genes in the wild type (WT) and *y11* mutant. A: Contents of δ -aminolevulinic acid (ALA) and porphobilinogen (PBG) in the second leaf of 14-day-old seedlings. B: Contents of uroporphyrinogen III (Urogen III), coproporphyrinogen III (Coprogen III), and protoporphyrin IX (Proto IX). C: Relative fluorescence of magnesium-protoporphyrin IX (Mg-Proto IX) and protochlorophyllide (Pchlde)

3.3 Disruption of Chloroplast Lamellae in the *yl1* Mutant

To explore the effect of reduced photosynthetic pigment contents on the chloroplast structure of the *yl1* mutant, the chloroplast ultrastructure was observed by transmission electron microscopy. Chloroplasts from WT leaves showed intact thylakoid and granum structure, with densely arranged grana lamellae (Figs. 4A and 4B). In contrast, chloroplast development was disrupted, and the grana lamellae were loose and disordered in the *yl1* mutant (Figs. 4C and 4D). It was speculated that the yellow leaf phenotype of the *yl1* mutant was caused by the decrease in photosynthetic pigment content resulting from impaired chloroplast development.

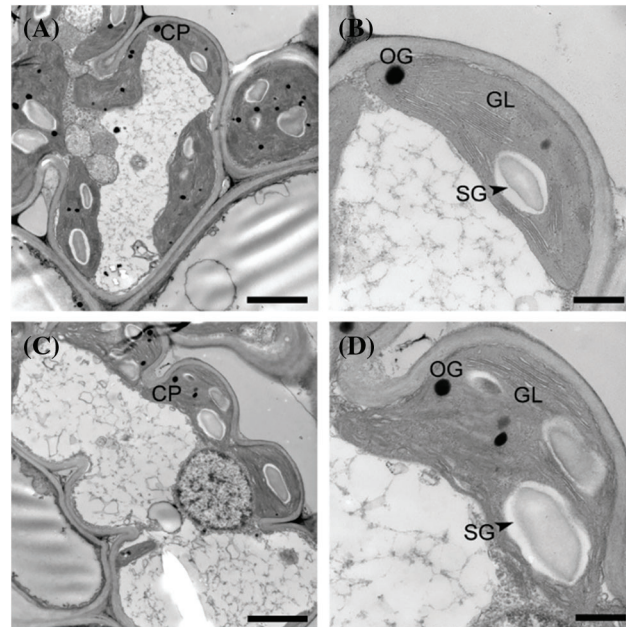


Figure 4: Ultrastructure of chloroplasts in the *yl1* mutant and wild type at the seedling stage. A and B: Transmission electron micrographs of chloroplasts of the wild type. C and D: Transmission electron micrographs of chloroplasts of the *yl1* mutant. A, C: bar = 2 μ m; B, D: bar = 500 nm. CP: chloroplast, OG: osmiophilic granule, GL: grana lamellae, SG: starch granule

3.4 Differential Gene Expression between the *yl1* Mutant and WT

To investigate the biological function of *yl1*, RNA-sequencing analysis was conducted to compare the transcriptome profiles of DEGs in the leaves of 4-week-old seedlings of the WT and *yl1* mutant. A total of 1,329 DEGs were identified between the *yl1* mutant and WT, of which 462 genes were up-regulated and 867 genes were down-regulated (Figs. 5A and 5C). These DEGs were distributed in all seven branches of KEGG metabolic pathways, such as metabolic pathways, genetic information processing pathways, and cell process pathways. All identified DEGs were clustered according to their biological roles. The GO enrichment of genes in the molecular function category were mainly significantly enriched for oxidoreductase activity and cofactor binding (Fig. 5B). The GO functional annotation was further divided into three components: molecular function, cellular component, and biological process. The highest number of genes was involved in the molecular function of catalytic activity, followed by an integral part of the cell and binding (Fig. 5D). KEGG pathway enrichment analysis revealed three significant KEGG pathways, comprising biosynthesis of secondary metabolites, phenylpropanoid biosynthesis, and starch and sucrose metabolism (Fig. 6). The changes in transcript abundance of genes involved in the chlorophyll and carotene synthesis and metabolism pathway and in chloroplast development between the *yl1* mutant and WT were further analyzed. The chlorophyll synthesis-related genes *OsCHLH*, *OsCHLM*,

OsCHLG, *PORB*, and *YGL8* were down-regulated in the *yl1* mutant, especially *OsCHLH*, *PORB*, and *YGL8* (Fig. 7A). These results indicated that the reduced chlorophyll content in the *yl1* mutant was caused by down-regulation of chlorophyll synthesis genes.

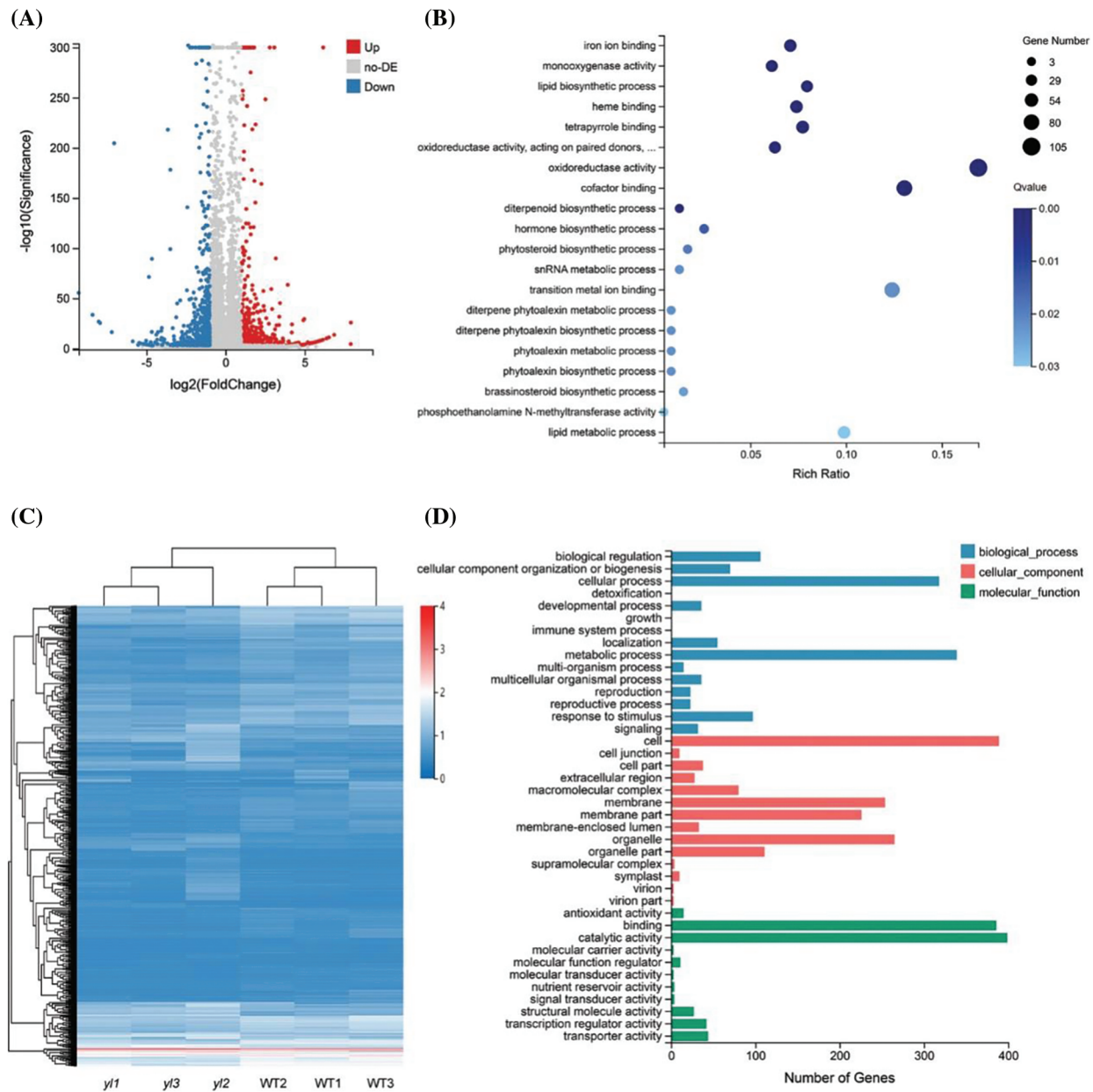


Figure 5: Transcriptional changes between the *yl1* mutant and wild type (WT). A: Volcano map of differentially expressed genes (DEGs) between the *yl1* mutant and WT. B: GO enrichment of DEGs between the *yl1* mutant and WT. C: Hierarchical cluster analysis of DEGs between the *yl1* mutant and WT. *yl1-yl3*, *yl1* mutant; WT1–WT3, wild type. D: GO functional classification of DEGs between the *yl1* mutant and WT

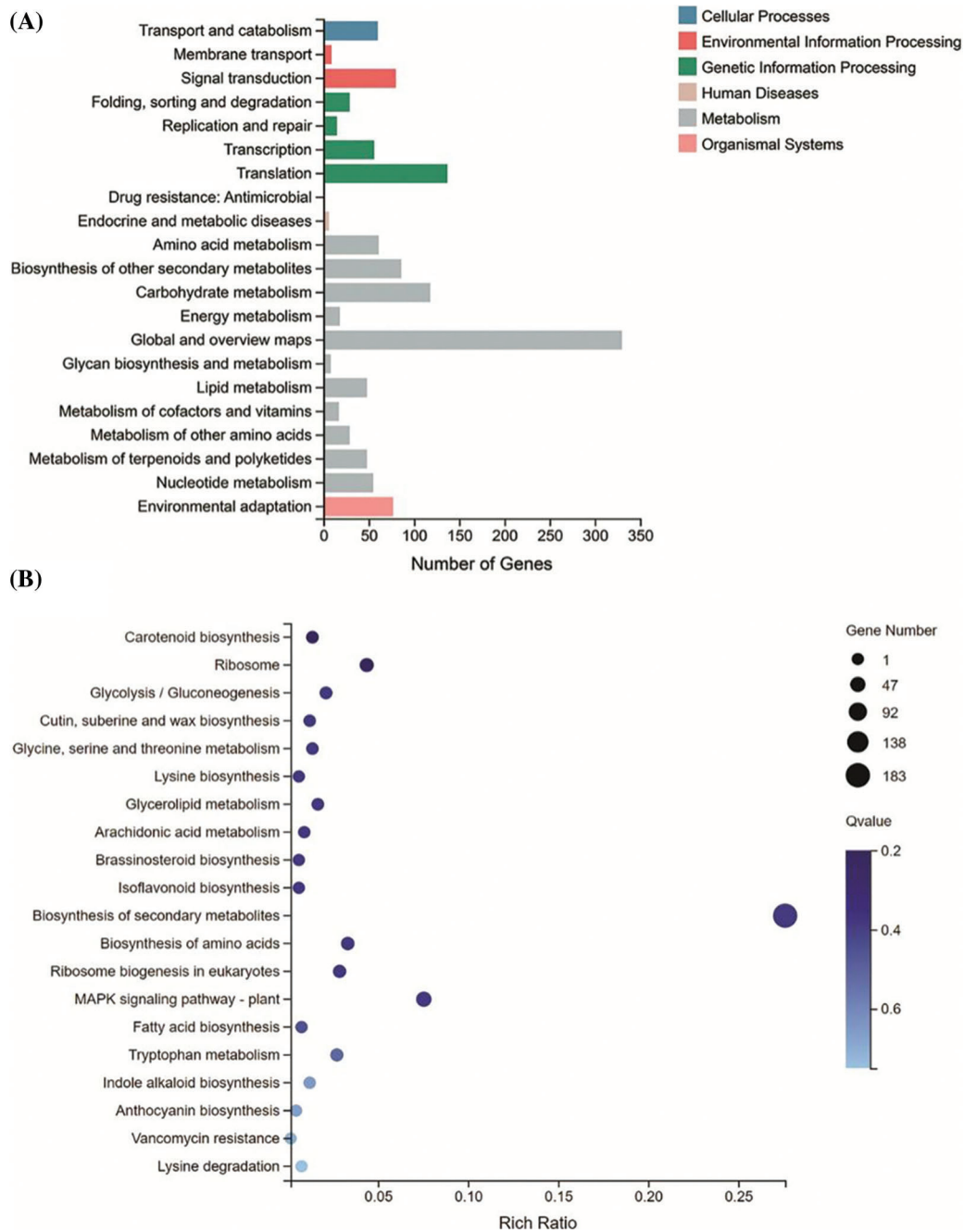


Figure 6: KEGG pathway functional classification and enrichment of differentially expressed genes (DEGs) between the wild type (WT) and *y11* mutant. A: KEGG functional classification of DEGs between the *y11* mutant and WT. B: KEGG enrichment of DEGs between the *y11* mutant and WT

To investigate further the effect of *y11* mutation on chloroplast development, we analyzed the expression of genes associated with chloroplast development in the WT and *y11* mutant. It was notable that the expression levels of the plastid division protein-encoding gene *FtsZ* and NEP core subunits-encoding gene *OsRpoTp* were significantly decreased in the *y11* mutant. The expression levels of the D1 protein of photosystem II (PsbA), PsaA (encoding the PsaA protein of photosystem I), and the large subunit of

ribulose-bisphosphate carboxylase/oxygenase (*RbcL*) were also significantly reduced in the *yl1* mutant (Fig. 7B). The expression of *ASL3* and *OsHAP3B* was increased in the *yl1* mutant (Fig. 7B). These results suggested that the mutation of *yl1* affected the levels of a broad range of mRNAs of imported precursors targeted to the chloroplast in rice.

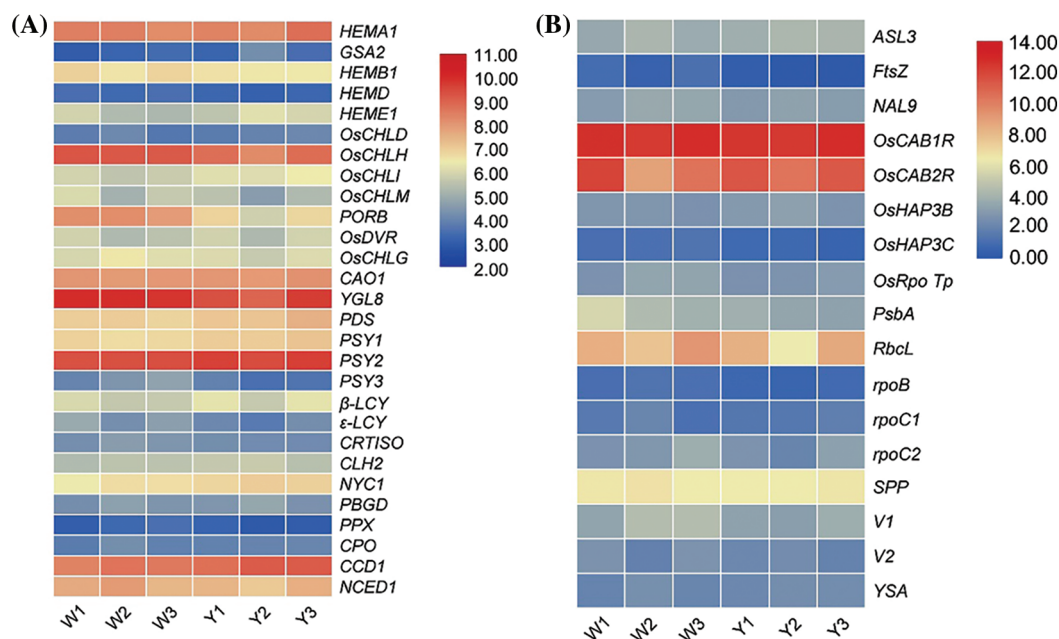


Figure 7: Relative expression of chlorophyll and carotene synthesis and metabolism-related genes (A) and chloroplast development-related genes (B) in the *yl1* mutant and wild type as indicated by RNA-sequencing analysis. Different genes are indicated by different colors. Relative expression levels are shown as a color gradient from low (blue) to high (red). W1–W3, wild type; Y1–Y3, *yl1* mutant

We further used qRT-PCR to analyze the expression of 10 genes involved in the chlorophyll biosynthetic pathway and chloroplast development pathway in rice. Compared with the WT, the *yl1* mutant displayed no difference in the expression levels of *OsCHLD* and *OsCHLI*, which encode the CHLD and CHLI subunits of Mg-chelatase, respectively. *OsCHLH*, which encodes the Mg-chelatase CHLH subunit, was significantly down-regulated. Expression of the chlorophyll biosynthetic genes *OsCHLG*, *OsCHLM*, *YGL8*, and *PORB* was also significantly down-regulated in the *yl1* mutant (Fig. 8). The chloroplast development-related genes *FtsZ*, *OsRpoTp*, and *RbcL* were also significantly down-regulated in the *yl1* mutant (Fig. 8). Overall, the results indicated that mutation of *yl1* affected the expression of genes associated with chloroplast development and resulted in the abnormal chloroplast structure observed in the *yl1* mutant.

3.5 Genetic Analysis and Map-Based Cloning of *yl1* Mutation Site

To analyze the genetic basis of the *yl1* mutation, crosses were performed using the *yl1* mutant as the female parent and two *indica* rice cultivars, ‘9311’ and ‘Yinguizhan’, as pollen donors. The leaf color of F₁ individuals and segregation ratios were investigated in the F₂ populations. All F₁ individuals displayed a green leaf phenotype identical to that of WT. The F₂ individuals derived from the crosses *yl1* × 9311 and *yl1* × Yinguizhan were separated into green leaf and yellow leaf phenotypes with a segregation ratio of 3:1 ($\chi^2 < \chi^2_{0.05} = 3.84, P > 0.05$) (Table 2). These results indicated that the leaf-color mutation of *yl1* was controlled by recessive nuclear gene.

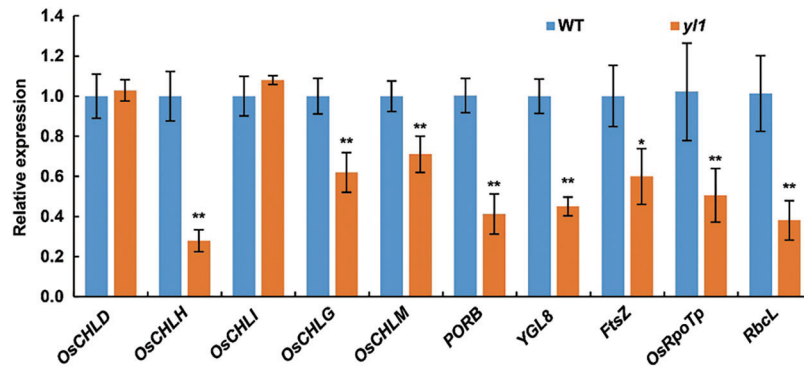


Figure 8: Relative expression levels of chlorophyll biosynthetic and chloroplast development genes. Data are means ($n = 3$), error bars indicate the SD. Asterisks indicate significant differences between the WT and *y11* mutant. * $P < 0.05$, ** $P < 0.01$

Table 2: Segregation of leaf color in F_2 population derived from crosses between the *y11* mutant and two green-leaved rice cultivars

Combination	Total No. of plants	No. of green leaf plants	No. of yellow leaf plants	Expected ratio	χ^2
<i>y11</i> /Yinguizhan	722	532	190	3:1	0.74
<i>y11</i> /9311	694	513	181	3:1	0.49

To map the chromosomal site of *y11*, another F_2 population was constructed by crossing the *y11* mutant with WT. The *y11* mutant and WT parents, and 20 green-leaved individuals and 20 yellow-leaved plants from the F_2 population were sequenced using an Illumina GAIIx DNA platform. We obtained 44.57 Gbp of short (75-bp) reads (Tables S2 and S3) that were aligned to the Nipponbare genome, resulting in identification of 2,759 SNP positions. For each SNP position, the value of the SNP index (the ratio of short reads harboring SNPs compared with the reference) was determined, and a graph relating SNP positions and the SNP index was generated for all 12 rice chromosomes. The causative SNP should be shared by all mutant F_2 plants and, therefore, have a SNP index = 1, whereas SNPs unrelated to the mutant phenotype should segregate in a 1:1 ratio among the F_2 progeny, resulting in a SNP index of 0.5. The MutMap approach applied to the F_2 progeny revealed a cluster of SNPs with high SNP index values, and that showed statistically significant deviations from the SNP index of 0.5 ($P < 0.01$), in the region between 17.34 Mb and 23.51 Mb on chromosome 3 (Fig. 9A). Sixteen SNPs with an SNP index of 1 were identified in the candidate region (Table 3). Among these 16 SNPs, 14 SNPs were located in the spacer region and two SNPs were located in the exon region, resulting in nonsynonymous mutations. Two SNPs at nucleotide positions 17,776,204 and 20,394,504 corresponded to the second exon of the genes *LOC_Os03g31210* and *LOC_Os03g36760*, and represented the nonsynonymous mutation of a proline (GCC) codon to a leucine (GCT) at residue 478 in *LOC_Os03g31210* and a lysine (AAA) codon to a glutamic acid (GAA) at residue 906 in *LOC_Os03g36760*, respectively (Table 3, Figs. 9B and 9D). We further confirmed the SNP presence in the genome using PCR and Sanger sequencing (Figs. 9C and 9E). *LOC_Os03g31210* encodes UDP-glucose 6-dehydrogenase, a crucial enzyme in the polysaccharide synthesis pathway, while *LOC_Os03g36760* encodes an expressed protein of unknown function with a plant mobile domain (PMD). Both of these genes have not been reported previously. In the UniProt database (<https://www.uniprot.org/uniprot/Q75GS4>), the function of *LOC_Os03g31210* is stated to produce UDP-glucuronic acid, which provides nucleotide sugars for cell-wall polymers. According to the Information Commons

for Rice Database (IC4R) (<http://ic4r.org/>) and transcriptomic database Rice eFP (<http://bar.utoronto.ca/efprice/cgi-bin/efpWeb.cgi>), *LOC_Os03g31210* expresses in the ovary and root, and *LOC_Os03g36760* widely expresses in various tissues (Fig. S1). Therefore, we concluded that *LOC_Os03g36760* was the *yl1* candidate gene.

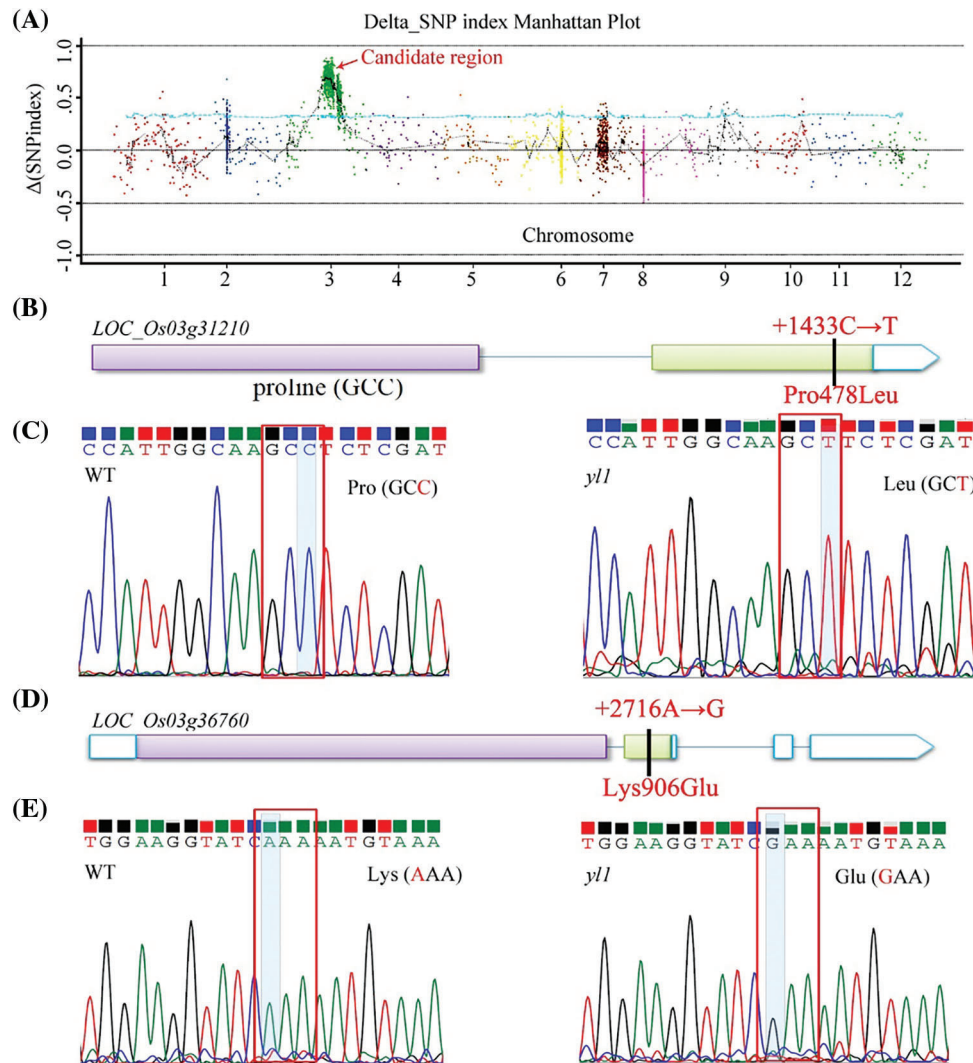


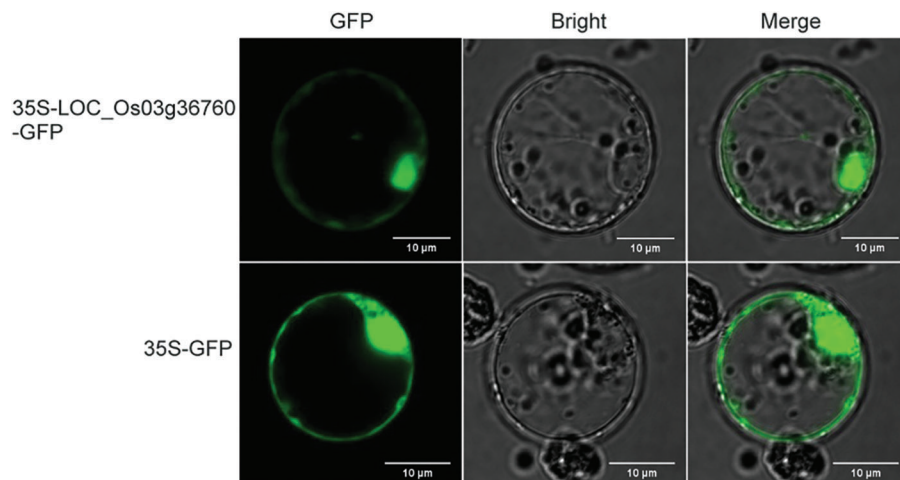
Figure 9: Identification of the *yl1* mutation using the MutMap method. A: SNP index plot of rice chromosome 3 generated by the MutMap analysis, showing a genomic region in which the highest SNP index peak harbored the candidate mutation. B: Gene structure and mutation sites in *LOC_Os03g31210*. C: Confirmation of the *yl1* mutation in *LOC_Os03g31210* by Sanger sequencing. A red box indicates the C-to-T transition. D: Gene structure and mutation sites in *LOC_Os03g36760*. E: Confirmation of the *yl1* mutation in *LOC_Os03g36760* by Sanger sequencing. A red box indicates the A-to-G transition

3.6 Subcellular Localization of *LOC_Os03g36760* Protein

To visualize the subcellular localization of *LOC_Os03g36760*, we fused *GFP* to the C-terminus of *LOC_Os03g36760*. The fluorescent signal of the *LOC_Os03g36760*-*GFP* fusion protein was detected in the nucleus, cytoplasm, and plasma membrane (Fig. 10).

Table 3: Candidate genes in mapping region of chromosome 3

Locus	SNP WT/yll	Gene ID	Variant	Putative function
Chr3: 17776204	C/T	<i>LOC_Os03g31210</i>	nonsynonymous	UDP-glucose 6-dehydrogenase, putative, expressed
Chr3: 20394504	A/G	<i>LOC_Os03g36760</i>	nonsynonymous	expressed protein
Chr3: 17346629	T/G	<i>LOC_Os03g30430</i>	upstream	nitrilase-associated protein, putative, expressed
Chr3: 17597434	G/A	/	intergenic	–
Chr3: 17668778	A/G	<i>LOC_Os03g31010</i>	upstream	expressed protein
Chr3: 18488802	C/T	<i>LOC_Os03g32314</i>	upstream	allene oxide cyclase 4, chloroplast precursor, putative, expressed
Chr3: 19204401	C/T	<i>LOC_Os03g33590</i>	upstream	interferon-related developmental regulator, putative, expressed
Chr3: 19717839	T/C	/	intergenic	–
Chr3: 19717916	A/G	/	intergenic	–
Chr3: 20019946	T/G	<i>LOC_Os03g36080</i>	upstream	expressed protein
Chr3: 20313054	C/T	<i>LOC_Os03g36630</i>	upstream	expressed protein
Chr3: 20391349	G/A	<i>LOC_Os03g36760</i>	upstream	expressed protein
Chr3: 20783015	C/T	<i>LOC_Os03g37470</i>	upstream	MATE efflux family protein, putative, expressed
Chr3: 21029852	C/G	<i>LOC_Os03g37864</i>	upstream	expressed protein
Chr3: 21352681	G/A	<i>LOC_Os03g38470</i>	upstream	GDSL-like lipase/acylhydrolase, putative, expressed
Chr3: 23513903	A/G	<i>LOC_Os03g42259</i>	upstream	hypervariable <i>Bacillus</i> group-specific protein, putative, expressed

**Figure 10:** Subcellular localization of the *LOC_Os03g36760* protein

4 Discussion

The leaf is the main organ for photosynthesis in plants. Chlorophyll plays a vital role in plant development and crop yield. The regulatory mechanism of chlorophyll synthesis and chloroplast structure is an important research focus in plant physiology and molecular biology. In recent years, the chlorophyll biosynthetic and degradative pathways have received much attention from plant physiologists and breeders [21]. Leaf-color mutants are important materials for studying photosynthesis, chlorophyll synthesis and degradation, and the regulatory mechanisms of growth and development, and are of high utility in hybrid seed production and biomass improvement of rice. In plants, chlorophyll biosynthesis begins with the precursor L-glutamyl-tRNA and involves a total of 15 steps. The entire synthesis pathway involves the participation of 15 enzymes and the expression of 27 genes encoding these enzymes [37]. Any obstacle encountered in this process may impair chlorophyll biosynthesis and result in leaf-color mutations [38]. The enzyme of Mg-chelatase catalyzes the insertion of Mg^{2+} into Proto IX to produce Mg-Proto IX. Reduced activity of Mg-chelatase may ultimately cause a decrease in chlorophyll synthesis [5]. In the *yll* mutant, the yellow leaf phenotype expressed at all growth stages. Compared with those in Lailong, the contents of chlorophyll *a* and chlorophyll *b* were significantly decreased in the *yll* mutant at the mature stage. Analysis of the contents of chlorophyll precursors showed that Proto IX accumulated, whereas Mg-Proto IX and Pchlide contents were significantly decreased, in the *yll* mutant (Figs. 3B and 3C), indicating that the synthesis of Mg-Proto IX from Proto IX in the mutant was blocked. In rice, *OsCHLH*, *OsCHLD*, and *OsCHLI* encode the ChlH, ChlD, and ChlI subunits of Mg-chelatase, respectively [4,5]. Compared with the WT, the *yll* mutant displayed no difference in expression of *OsCHLD* and *OsCHLI*, whereas *OsCHLH* was significantly down-regulated (Fig. 8). Previous studies have shown that mutations and down-regulation of *OsCHLH* may cause a decrease in leaf chlorophyll content, resulting in yellow leaf phenotypes [4]. Therefore, we concluded that the decreased expression of *OsCHLH* resulted in the blocked synthesis of Mg-Proto IX, which caused the reduced chlorophyll contents in leaves of the *yll* mutant.

Chloroplast differentiation and development are controlled by the interaction and co-regulation of nuclear genes and plastid genes [39]. This differentiation and development process can be divided into seven steps, and any obstructed pathway leads to chloroplast hypoplasia, thus affecting plant chlorophyll content and causing leaf-color mutations [38,40]. *FtsZ* encodes a plastid division protein that plays an important role in chloroplast division [41–43]. In the *yll* mutant, the expression levels of *FtsZ*, *RbcL*, and *OsRpoTp* were significantly decreased (Fig. 8), whereas those of *ASL3* and *OsHAP3B* were increased (Fig. 7). Overall, these results suggested that the mutation of *yll* affected the expression of genes associated with chloroplast development, and thereby caused the abnormal chloroplast structure in the *yll* mutant. Impairment of chloroplast development affects the photosynthetic efficiency of plants. This impairment then reduces the photosynthetic efficiency of chloroplast-related mutants and reduced plant yield. In addition, mutations causing deficiency in the capability to synthesize chlorophyll, including the genes *OsCHLH*, *OsCHLD*, *OsCHLI*, *OsCHLG*, and *YGL8*, also reduce yield to varying degrees [4,5,7,44,45]. In the *yll* mutant, the chlorophyll content and expression of chlorophyll synthesis-related genes were decreased, and the chloroplasts exhibited abnormal morphology, with loose thylakoid membranes and disordered grana lamellae. Compared with Lailong, grain number per spike, 1000-grain weight, and plant height in the *yll* mutant were all reduced. Therefore, we considered that the mutation of *yll* caused abnormal chloroplast development and blocked chlorophyll synthesis in rice, which ultimately affected yield-related traits of the *yll* mutant.

At present, more than 120 rice leaf color-related genes have been cloned and are distributed on the 12 chromosomes of rice, of which chromosome 3 harbors the highest number of cloned genes. Genes associated with chlorophyll synthesis, including *OsCHLH*, *OsCHLD*, *OsCHLI*, *NOL*, *PAO*, and *OsDVR*, are all located on chromosome 3. These results suggest that a mutation hotspot region for chlorophyll

content may exist on chromosome 3 in rice. In this study, using the MutMap method, we mapped the *yl1* gene located near the centromeric region of chromosome 3, and identified two previously unreported non-synonymous SNPs located in *LOC_Os03g31210* and *LOC_Os03g36760*. *LOC_Os03g36760* encodes a protein of unknown function with a PMD. The PMD proteins are ubiquitous in plants. A previous phylogenetic analysis of the PMD family indicated that *LOC_Os03g36760*, together with two other rice PMD proteins and eight *Arabidopsis* PMD proteins, was placed in the PMD-B clade and associated with PCGs [46]. The PMD-A clade proteins in *Arabidopsis* define an alternative silencing pathway independent of DNA methylation and short interfering RNAs [46]. However, the function of PMD-B clade proteins in *Arabidopsis* and rice has not been reported. Therefore, the function of *LOC_Os03g36760* requires further study.

5 Conclusion

A yellow leaf rice mutant, *yl1*, was identified from the EMS-treated progeny of Lailong, a rice landrace cultivated in Guizhou. The yellow leaf phenotype of *yl1* was caused by abnormal chloroplast development and inhibition of chlorophyll synthesis. Genetic analysis revealed that the yellow leaf phenotype of the *yl1* mutant was controlled by a single recessive gene. By employing the MutMap method, two non-synonymous SNPs located in *LOC_Os03g31210* and *LOC_Os03g36760* were identified. *LOC_Os03g36760* may be the candidate gene for the *yl1* mutant. These results will be useful for further characterization and cloning of *yl1*, and for research on the molecular mechanisms controlling biogenesis and chloroplast biochemical processes.

Authorship: Z. X. F., L. G. Z., L. N. A, L. Y., H. X. Z. and L. J. R. assisted in the experiments. Z. X. F wrote the manuscript. Z. X. F and Z. D. G. supervised the research.

Funding Statement: This work was supported by grants from the Guizhou Province High-Level Innovative Talent Training Program Project ([2016]4003), the Guizhou Science and Technology Major Project [20126005] and the Guizhou Science and Technology Project (20171039).

Conflicts of Interest: The authors declare that they have no conflicts of interest to report regarding the present study.

References

1. Wang, W., Gao, H., Liang, Y., Li, J., Wang, Y. (2022). Molecular basis underlying rice tiller angle: Current progress and future perspectives. *Molecular Plant*, 15(1), 125–137. DOI 10.1016/j.molp.2021.12.002.
2. Khush, G. S. (2005). What it will take to Feed 5.0 Billion Rice consumers in 2030. *Plant Molecular Biology*, 59(1), 1–6. DOI 10.1007/s11103-005-2159-5.
3. Singh, U., Prithiviraj, B., Sarma, B. (2000). Development of *Erysiphe pisi* (powdery mildew) on normal and albino mutants of pea (*Pisum sativum* L.). *Journal of Phytopathology*, 148(11–12), 591–595. DOI 10.1046/j.1439-0434.2000.00558.x.
4. Jung, K. H., Hur, J., Ryu, C. H., Choi, Y., Chung, Y. Y. et al. (2003). Characterization of a rice chlorophyll-deficient mutant using the T-DNA gene-trap system. *Plant and Cell Physiology*, 44(5), 463–472. DOI 10.1093/pcp/pcg064.
5. Zhang, H., Li, J., Yoo, J. H., Yoo, S. C., Cho, S. H. et al. (2006). Rice *Chlorina-1* and *Chlorina-9* encode ChlD and ChlI subunits of Mg-chelatase, a key enzyme for chlorophyll synthesis and chloroplast development. *Plant Molecular Biology*, 62(3), 325–337. DOI 10.1007/s11103-006-9024-z.
6. Deng, X. J., Zhang, H. Q., Wang, Y., He, F., Liu, J. L. et al. (2014). Mapped clone and functional analysis of leaf-color gene *Ygl7* in a rice hybrid (*Oryza sativa* L. ssp. *indica*). *PLoS One*, 9(6), e99564. DOI 10.1371/journal.pone.0099564.
7. Lee, S., Kim, J. H., Yoo, E. S., Lee, C. H., Hirochika, H. et al. (2005). Differential regulation of *chlorophyll a* oxygenase genes in rice. *Plant Molecular Biology*, 57(6), 805–818. DOI 10.1007/s11103-005-2066-9.

8. Wang, P., Gao, J., Wan, C., Zhang, F., Xu, Z. et al. (2010). Divinyl chlorophyll(ide) a can be converted to monovinyl chlorophyll(ide) a by a divinyl reductase in rice. *Plant Physiology*, *153*(3), 994–1003. DOI 10.1104/pp.110.158477.
9. Wang, Q., Zhu, B., Chen, C., Yuan, Z., Guo, J. et al. (2021). A single nucleotide substitution of *GSAM* gene causes massive accumulation of glutamate 1-semialdehyde and yellow leaf phenotype in rice. *Rice*, *14*(1), 50. DOI 10.1186/s12284-021-00492-x.
10. Liu, X., Huang, Q., Yang, Y., Tang, J., Zhao, Y. et al. (2021). Characterization and map-based cloning of the novel rice yellow leaf mutant *yl3*. *Journal of Plant Biology*, *64*(1), 35–44. DOI 10.1007/s12374-020-09275-1.
11. Goh, C. H., Satoh, K., Kikuchi, S., Kim, S. C., Ko, S. M. et al. (2010). Mitochondrial activity in illuminated leaves of chlorophyll-deficient mutant rice (*OsCHLH*) seedlings. *Plant Biotechnology Reports*, *4*(4), 281–291. DOI 10.1007/s11816-010-0146-z.
12. Wang, X., Huang, R., Quan, R. (2017). Mutation in Mg-Protoporphyrin IX monomethyl ester cyclase decreases photosynthesis capacity in rice. *PLoS One*, *12*(1), e0171118. DOI 10.1371/journal.pone.0171118.
13. Yang, Y., Xu, J., Huang, L., Leng, Y., Dai, L. et al. (2016). *PGL*, encoding chlorophyllide a oxygenase 1, impacts leaf senescence and indirectly affects grain yield and quality in rice. *Journal of Experimental Botany*, *67*(5), 1297–1310. DOI 10.1093/jxb/erv529.
14. Sakuraba, Y., Rahman, M. L., Cho, S. H., Kim, Y. S., Koh, H. J. et al. (2013). The rice *faded green leaf* locus encodes protochlorophyllide oxidoreductase B and is essential for chlorophyll synthesis under high light conditions. *Plant Journal*, *74*(1), 122–133. DOI 10.1111/tbj.12110.
15. Cai, L., Liu, J., Yun, H., Du, D., Zhong, X. et al. (2021). Characterization and candidate gene analysis of the yellow-green leaf mutant *ygl16* in rice (*Oryza sativa* L.). *Phyton-International Journal of Experimental Botany*, *90*(4), 1103–1117. DOI 10.32604/phyton.2021.015532.
16. Dong, H., Fei, G. L., Wu, C. Y., Wu, F. Q., Sun, Y. Y. et al. (2013). A rice *virescent-yellow leaf* mutant reveals new insights into the role and assembly of plastid caseinolytic protease in higher plants. *Plant Physiology*, *162*(4), 1867–1880. DOI 10.1104/pp.113.217604.
17. Li, W., Wu, C., Hu, G., Xing, L., Qian, W. et al. (2013). Characterization and fine mapping of a novel rice narrow leaf mutant *nal9*. *Journal of Integrative Plant Biology*, *55*(11), 1016–1025. DOI 10.1111/jipb.12098.
18. Yoo, S. C., Cho, S. H., Sugimoto, H., Li, J., Kusumi, K. et al. (2009). Rice *virescent3* and *stripe1* encoding the large and small subunits of ribonucleotide reductase are required for chloroplast biogenesis during early leaf development. *Plant Physiology*, *150*(1), 388–401. DOI 10.1104/pp.109.136648.
19. Yang, Q., He, H., Li, H., Tian, H., Zhang, J. et al. (2011). *NOA1* functions in a temperature-dependent manner to regulate chlorophyll biosynthesis and Rubisco formation in rice. *PLoS One*, *6*(5), e20015. DOI 10.1371/journal.pone.0020015.
20. Liu, H., Lau, E., Lam, M. P. Y., Chu, H., Li, S. et al. (2010). *OsNOA1/RIF1* is a functional homolog of *AtNOA1/RIF1*: Implication for a highly conserved plant cGTPase essential for chloroplast function. *New Phytologist*, *187*(1), 83–105. DOI 10.1111/j.1469-8137.2010.03264.x.
21. Liu, W., Fu, Y., Hu, G., Si, H., Zhu, L. et al. (2007). Identification and fine mapping of a thermo-sensitive chlorophyll deficient mutant in rice (*Oryza sativa* L.). *Planta*, *226*(3), 785–795. DOI 10.1007/s00425-007-0525-z.
22. Lin, D., Jiang, Q., Zheng, K., Chen, S., Zhou, H. et al. (2015). Mutation of the rice *ASL2* gene encoding plastid ribosomal protein L21 causes chloroplast developmental defects and seedling death. *Plant Biology*, *17*(3), 599–607. DOI 10.1111/plb.12271.
23. Yoo, J. H., Park, J. H., Cho, S. H., Yoo, S. C., Li, J. et al. (2011). The rice *bright green leaf (bgl)* locus encodes *OsRopGEF10*, which activates the development of small cuticular papillae on leaf surfaces. *Plant Molecular Biology*, *77*(6), 631–641. DOI 10.1007/s11103-011-9839-0.
24. Moon, S., Giglione, C., Lee, D. Y., An, S., Jeong, D. H. et al. (2008). Rice peptide deformylase *PDF1B* is crucial for development of chloroplasts. *Plant and Cell Physiology*, *49*(10), 1536–1546. DOI 10.1093/pcp/pcn121.
25. Krishnan, A., Guiderdoni, E., An, G., Yue-Ie, C. H., Han, C. D. et al. (2009). Mutant resources in rice for functional genomics of the grasses. *Plant Physiology*, *149*(1), 165–170. DOI 10.1104/pp.108.128918.

26. Zhu, Y., Yan, P., Dong, S., Hu, Z., Wang, Y. et al. (2021). Map-based cloning and characterization of *YGL22*, a new yellow-green leaf gene in rice (*Oryza sativa*). *Crop Science*, *61*(1), 529–538. DOI 10.1002/csc2.20347.
27. Arnon, D. I. (1949). Copper enzymes in isolated chloroplasts. polyphenoloxidase in *Beta Vulgaris*. *Plant Physiology*, *24*(1), 1–15. DOI 10.1104/pp.24.1.1.
28. Morton, R. A. (1975). Biochemical spectroscopy. London: Adam Hilger. DOI 10.1016/0076-6879(95)46007-1.
29. Santiago-Ong, M., Green, R. M., Tingay, S., Brusslan, J. A., Tobin, E. M. (2001). *shygrll* is a mutant affected in multiple aspects of photomorphogenesis. *Plant Physiology*, *126*(2), 587–600. DOI 10.1104/pp.126.2.587.
30. Masuda, T., Fusada, N., Oosawa, N., Takamatsu, K. I., Yamamoto, Y. Y. et al. (2003). Functional analysis of isoforms of NADPH: Protochlorophyllide OXIDOREDUCTASE (POR), PORB and PORC, in *Arabidopsis thaliana*. *Plant and Cell Physiology*, *44*(10), 963–974. DOI 10.1093/pcp/pcg128.
31. Wang, L., Feng, Z., Wang, X., Wang, X., Zhang, X. (2009). DEGseq: An R package for identifying differentially expressed genes from RNA-seq data. *Bioinformatics*, *26*(1), 136–138. DOI 10.1093/bioinformatics/btp612.
32. Li, Y., Huang, R., Li, J., Huang, X., Zeng, X. et al. (2020). *DWARF* and *SMALL SEED1*, a novel allele of *OsDWARF*, controls rice plant architecture, seed size, and chlorophyll biosynthesis. *Phyton-International Journal of Experimental Botany*, *90*(1), 111–127. DOI 10.32604/phyton.2020.013933.
33. Livak, K. J., Schmittgen, T. D. (2001). Analysis of relative gene expression data using Real-Time quantitative PCR and the $2^{-\Delta\Delta CT}$ method. *Methods*, *25*(4), 402–408. DOI 10.1006/meth.2001.1262.
34. Abe, A., Kosugi, S., Yoshida, K., Natsume, S., Takagi, H. et al. (2012). Genome sequencing reveals agronomically important loci in rice using MutMap. *Nature Biotechnology*, *30*(2), 174–178. DOI 10.1038/nbt.2095.
35. Li, R., Yu, C., Li, Y., Lam, T. W., Yiu, S. M. et al. (2009). SOAP2: An improved ultrafast tool for short read alignment. *Bioinformatics*, *25*(15), 1966–1967. DOI 10.1093/bioinformatics/btp336.
36. Li, H., Sun, H., Jiang, J., Sun, X., Tan, L. et al. (2021). *TAC4* controls tiller angle by regulating the endogenous auxin content and distribution in rice. *Plant Biotechnology Journal*, *19*(1), 64–73. DOI 10.1111/pbi.13440.
37. Beale, S. I. (2005). Green genes gleaned. *Trends in Plant Science*, *10*(7), 309–312. DOI 10.1016/j.tplants.2005.05.005.
38. Zhao, M. H., Li, X., Zhang, X. X., Zhang, H., Zhao, X. Y. (2020). Mutation mechanism of leaf color in plants: A review. *Forests*, *11*(8), 851. DOI 10.3390/f11080851.
39. Chan, K. X., Crisp, P. A., Estavillo, G. M., Pogson, B. J. (2010). Chloroplast-to-nucleus communication. *Plant Signaling & Behavior*, *5*(12), 1575–1582. DOI 10.4161/psb.5.12.13758.
40. Pogson, B. J., Albrecht, V. (2011). Genetic dissection of chloroplast biogenesis and development: An overview. *Plant Physiology*, *155*(4), 1545–1551. DOI 10.1104/pp.110.170365.
41. Vitha, S., McAndrew, R. S., Osteryoung, K. W. (2001). FtsZ ring formation at the chloroplast division site in plants. *Journal of Cell Biology*, *153*(1), 111–120. DOI 10.1083/jcb.153.1.111.
42. Glynn, J. M., Yang, Y., Vitha, S., Schmitz, A. J., Hemmes, M. et al. (2009). PARC6, a novel chloroplast division factor, influences FtsZ assembly and is required for recruitment of PDV1 during chloroplast division in *Arabidopsis*. *Plant Journal*, *59*(5), 700–711. DOI 10.1111/j.1365-313X.2009.03905.x.
43. Liu, X., An, J., Wang, L., Sun, Q., An, C. et al. (2021). A novel amphiphilic motif at the C-terminus of FtsZ1 facilitates chloroplast division. *Plant Cell*, *34*(1), 419–432. DOI 10.1093/plcell/koab272.
44. Wu, Z., Zhang, X., He, B., Diao, L., Sheng, S. et al. (2007). A chlorophyll-deficient rice mutant with impaired chlorophyllide esterification in chlorophyll biosynthesis. *Plant Physiology*, *145*(1), 29–40. DOI 10.1104/pp.107.100321.
45. Zhu, X., Guo, S., Wang, Z., Du, Q., Xing, Y. et al. (2016). Map-based cloning and functional analysis of *YGL8*, which controls leaf colour in rice (*Oryza sativa*). *BMC Plant Biology*, *16*(1), 134. DOI 10.1186/s12870-016-0821-5.
46. Ikeda, Y., Pélissier, T., Bourguet, P., Becker, C., Pouch-Pélissier, M. N. et al. (2017). *Arabidopsis* proteins with a transposon-related domain act in gene silencing. *Nature Communications*, *8*(1), 15122. DOI 10.1038/ncomms15122.

Supplementary Materials

Table S1: Primer used in this work

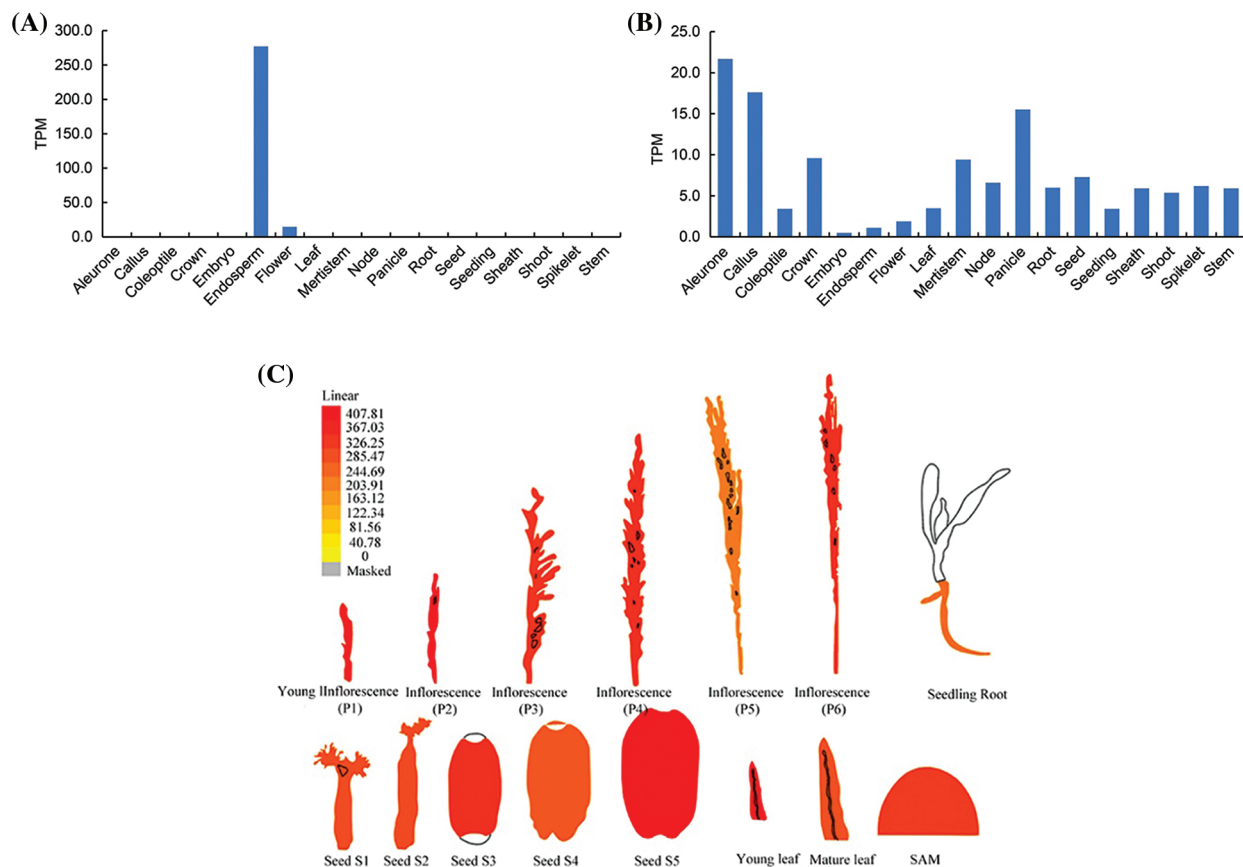
Primers	Primer sequences	Purpose
<i>LOC_Os03g31210-F</i>	5'-GCGTCTGCATCCTCACTG-3'	Gene SNP test
<i>LOC_Os03g31210-R</i>	5'-AACAACCCATTCCCTCCA-3'	
<i>LOC_Os03g36760-F</i>	5'-AAAGATGTTAGGGTCCAA-3'	Gene SNP test
<i>LOC_Os03g36760-R</i>	5'-AAGTTCCTTCATCGGTAG-3'	
<i>OsCHLD-F</i>	5'-GCTCAGCAAGCTCAAAGA-3'	Real-time PCR
<i>OsCHLD-R</i>	5'-ACCCTTGGGAAGCATAGA-3'	
<i>OsCHLI-F</i>	5'-GTCCTACTTGGAGGAACAAGAC-3'	Real-time PCR
<i>OsCHLI-R</i>	5'-TCAACTCTGCACACTTTAGA-3'	
<i>OsCHLH-F</i>	5'-AACTGGATGAGCCAGAAGAGA-3'	Real-time PCR
<i>OsCHLH-R</i>	5'-AAATGCAAAAGACTTGCGACT-3'	
<i>OsCHLG-F</i>	5'-GGTCCATGTCTTACAGGATACAC-3'	Real-time PCR
<i>OsCHLG-R</i>	5'-GATATAGCGCCTGAAGGAATAG-3'	
<i>OsCHLM-F</i>	5'-AGGACGCTCTACTTCGACTTC-3'	Real-time PCR
<i>OsCHLM-R</i>	5'-TAGAACTGCGTGGAGATGAAGC-3'	
<i>Ftzs-F</i>	5'-CCGGATCACTGCGATTACGA-3'	Real-time PCR
<i>Ftzs-R</i>	5'-GCCGCATTCATCCCAATGTC-3'	
<i>RbcL-F</i>	5'-GTCTACGCGGTGGACTTGAT-3'	Real-time PCR
<i>RbcL-R</i>	5'-CGCGGCAATAATGAGCCAAA-3'	
<i>YGL8-F</i>	5'-GAGCCCCAGCTTGTCTACTG-3'	Real-time PCR
<i>YGL8-R</i>	5'-TCATCTCACCGTTCGAAGCC-3'	
<i>PORB-F</i>	5'-AGGACGCGTTTCTCACGAAT-3'	Real-time PCR
<i>PORB-R</i>	5'-CCCATCCCATGATCCACCAG-3'	
<i>OsRpoTp-F</i>	5'-ATGGGGCACAGAATCCCAAG-3'	Real-time PCR
<i>OsRpoTp-R</i>	5'-GGTATCTCCACGTGCCTAGC-3'	
<i>OsActin1-F</i>	5'-TGACGGAGCGTGGTTACTCATTCA-3'	Real-time PCR
<i>OsActin1-R</i>	5'-TCTTGGCAGTCTCCATTTCTGGT-3'	

Table S2: Summary of blast results of green leaf and yellow leaf individuals from F₂ population, WT and *yll* aligned and Nipponbare reference genome

Sample	Raw base (bp)	Clean base (bp)	Effective rate (%)	Error rate (%)	Q20 (%)	Q30 (%)	GC content (%)
WT	9,303,036,300	9,281,211,600	99.77	0.03	96.03	93.66	43.88
<i>yll</i>	8,991,929,100	8,969,342,400	99.75	0.03	96.06	93.68	43.93
green	15,465,509,700	15,435,310,800	99.81	0.03	95.60	93.05	43.88
yellow	10,807,953,600	10,783,533,000	99.77	0.03	95.61	93.25	43.65

Table S3: Summary of original sequencing data and mapping statistics on the genome aligned and Nipponbare reference genome

Sample	Mapped reads	Total reads	Mapping rate (%)	Average depth (X)	Coverage at least 1X (%)	Coverage at least 4X (%)
WT	60,829,681	61,874,744	98.31	22.45	96.47	95.10
<i>y11</i>	58,849,633	59,795,616	98.42	21.75	96.41	95.00
green	101,233,325	102,902,072	98.38	36.93	97.50	95.87
yellow	70,809,805	71,890,220	98.50	26.60	96.56	95.32

**Figure S1:** The expression levels in various tissues A: The gene expression levels of *LOC_Os03g31210* in various tissues in Information Commons for Rice Database (IC4R); B: The gene expression levels of *LOC_Os03g36370* in various tissues in Information Commons for Rice Database (IC4R); C: The gene expression levels of *LOC_Os03g36370* in various tissues in transcriptomic database Rice eFP